

Novel mesophase behavior in two-dimensional binary solid solutions

B.P. Prajwal and Fernando A. Escobedo*

Department of Chemical and Biomolecular Engineering, Cornell University, Ithaca, New York 14853, USA

Abstract

Monte Carlo simulations were used to study the assembly of binary mixtures of hard disks with either squares or hexagons, where the components have size ratios that optimize their co-assembly into compositionally disordered solids. For the disks+squares mixtures, along with the enhanced regions of solid miscibility, a continuous-looking transition from the disk-like to the square-like behavior occurred through a novel mosaic (M) phase, which seamlessly bridges the hexatic and tetratic mesophase regions. The M phase has interspersed tetratic, hexatic, and rhombic-like locally ordered clusters. For the disks+hexagons mixture, fully mixed hexatic mesophase was observed for all compositions.

Recent advances in the synthesis [1–3] and fabrication [4,5] of faceted sub-micron particles with different shapes have spurred interest in their use as building blocks for the assembly of targeted complex structures. Several tunable parameters like particle shape [6,7] and inter-particle interactions (chemical *patchiness*) [7,8], allow the design of a wide range of morphologies and material properties having enhanced optical characteristics for potential applications in nanophotonics [9,10], sensors [11], and catalysis [12–14]. Towards designing new complex materials, recent efforts have focused on predicting phase behavior using theoretical [15,16] and simulation techniques [6,17–21] for hard polyhedral particles in the bulk (3D) and in monolayers (2D), where the formation of ordered structures entirely depends on the entropic forces encoded in the particle shape. Monolayer (2D) superstructures are of particular importance, as several experimental protocols leveraging slit confinement or interfacial pinning [22,23] can be deployed to assemble monolayers from different readily synthesizable nano- and micro-sized polyhedral or polygonal particles for applications in thin-film optical and electronic devices [24–28].

Single-component hard-particle superstructures arise at sufficiently high concentrations due to packing entropy manifesting as effective entropic bonds between the constituent particles, which favors particular arrangements. It has been reported that both the pure systems of squares and of hexagons exhibit a Kosterlitz-Thouless-Halperin-Nelson-Young (KTHNY) behavior, wherein the transition is continuous between isotropic fluid and tetratic phase for squares, and between fluid and hexatic phase for hexagons, and a continuous transition from the appropriate (n -fold)-atic (where $n=4$ for squares, 6 for hexagons) phase to the solid phase [21]. The tetratic and hexatic phases are partially ordered mesophases characterized by a short-range translational order and quasi-long/long-range bond orientational order. Simulation results reported for the melting behavior of hard disks suggest that the transition occurs in two steps with a first-order fluid-hexatic transition and a continuous hexatic-solid phase transition [29].

By ‘*mixing*’ particles of different shapes (and chemistries), we can broaden our space of exploration to access a wider variety of superstructures having a combination of the constituents’ physical properties. For example, ordered superstructures have been predicted for binary mixtures of hexagons+squares, squares+triangles, hexagons+triangles with and without enthalpic patchiness encoded in their facets [30]. The phase behavior of binary mixtures strongly depends on the relative size ratios and contents of the components. This correlation was observed in a size-bidisperse system of hard disks, where the liquid-hexatic-solid transition changes to a first order liquid-solid transition upon increasing the composition of the small disks [31]. For binary mixtures of parallel hard squares having disparate sizes, a fluid-solid phase-separated state was found with small and large squares forming the fluid and solid phases, respectively [32]. These predicted phases are thermodynamically stabilized by the interplay of mixing and packing entropy (that favors efficient packing of the components). At very high pressures, packing entropy dominates over mixing entropy leading to strong segregation of the components into their respective stable structures.

The focus of this paper is to explore the phase behavior of 2D hard binary mixtures of disks+squares and disks+hexagons, when the components have size ratios that optimize their co-assembly into solid solutions. The size ratio is defined as $\xi = \sigma/a$ where σ = disk diameter and a = polygon edge length. For this purpose, we adopted the exchange free-energy method [33] to predict ξ values which tend to maximize the range of compositions and packing fractions where

substitutionally disordered solid solutions occur. This approach, intended to have general applicability, was shown to be a robust metric for estimating the optimal ξ in binary mixtures of spheres and polyhedra to form substitutionally disordered 3D solid solutions [33]. The method is based on estimating an exchange free-energy (ΔF_x) metric, by probing the environment of the individual component solid phases with a guest particle. For two pure solid phases s_i and s_j of components i and j , ΔF_x is obtained by adding the excess chemical potentials associated with “exchanging” a host particle into a guest particle:

$$\Delta F_x = \mu_{ex}^{s_i}(i \rightarrow j) + \mu_{ex}^{s_j}(j \rightarrow i) \quad (1)$$

where $\mu_{ex}^{s_i}(i \rightarrow j)$ (or $\mu_{ex}^{s_j}(j \rightarrow i)$) is the reduced excess chemical potential (in units of thermal energy) associated with virtually mutating one particle of type i (or j) into a particle of type j (or i) in pure phase s_i (or s_j) at the pressure p_m (the smallest pressure at which both pure components are solid phases for a given ξ). ΔF_x was obtained for a range of ξ values of interest, and the ξ value corresponding to the minimum value of ΔF_x , representing a minimal “cost” for host-guest substitutions in both solid phases, is considered optimal for enhancing the mixing entropy and promoting substitutionally disordered solid solutions. The connection between ΔF_x and mixing entropy/free-energy is discussed in the Supplementary Information (SI, Sec. I).

For the disk+square mixture, a novel mosaic (M) phase is found having locally ordered microscopic clusters with square-rich four-fold and rhombic (RB) lattice symmetry, and disk-rich six-fold symmetry, that are distributed randomly throughout the simulated domain. This unique behavior of coexisting finite clusters of two different symmetries (six and four-fold) can be seen as a mesophase bridging the hexatic and tetratic mesophases observed for the disk-rich and square-rich systems, respectively. For the hexagons+disks mixtures, the hexatic phase is observed for all compositions since the individual pure-components have similar order-disorder transition behavior and lattice symmetry.

We verified the formation of solid solutions by mapping the pressure-composition phase diagrams using hard-particle Monte Carlo simulations in the isothermal-isobaric ensemble (see SI Sec. II) for the binary-mixtures having *optimized* components size ratio ξ values (1.1 for disks+squares and 1.82 for disks+hexagons, see SI Sec. III). The phase boundaries were identified by analyzing the local correlation of the six-fold and four-fold bond-orientational (see SI Sec. IV for details)

and the positional order parameters. At high pressures, the mixtures phase separate into their respective nearly pure component solid phases. The regions where the two phases coexist were mapped based on the results from interfacial simulations (see SI Sec. II). Most interfacial simulations were carried out at the equimolar global composition, with additional runs performed for other compositions to better map out the two-phase coexistence boundaries. Results are reported in the following dimensionless quantities: distance, $r^* = r/a$, reduced pressure, $P^* = Pa^2/k_bT$ and area fraction/density, $\eta = NA_p/A$, where P is the pressure, k_b is Boltzmann's constant, T is temperature, a is the edge of the polygon, N is the total number for particles, A is the total area of the system, and A_p is the area occupied by the particles.

The disks and hexagons form a ‘compatible’ mixture system, since both pure-components form the hexatic and 1Δ ordered phases. This enables a high mixing affinity that leads to the formation of a 1Δ solid solution for the entire range of hexagon compositions, x_h as seen in Fig. 1. The hexatic mesophase was also stable for all compositions for $2.72 < P^* < 2.76$ in the disk-rich and $2.66 < P^* < 2.73$ in the hexagon-rich regions. We identified the boundaries between the hexatic mesophase and 1Δ solid solution by analyzing the positional pair-correlation and six-fold bond orientational correlation functions (see SI Sec. VI). We note that two- 1Δ phase-separated states would be expected to occur at pressures much larger than those simulated here.

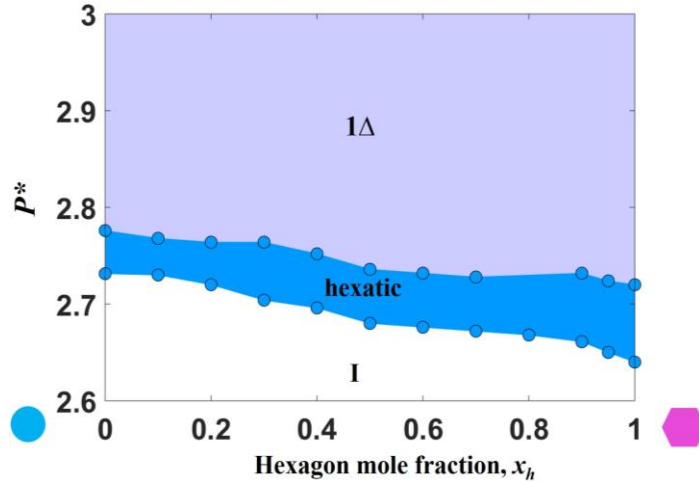


FIG. 1 (color online). Pressure-composition phase diagram for mixtures of disks+hexagons for optimal component size ratio, $\zeta = 1.82$. The symbol 1Δ denote the triangular solid phase.

The pressure-composition (Fig. 2a) and area fraction-composition (Fig. 2b) phase diagrams for the disks+squares mixture exhibit broad stable regions of substitutionally disordered square-rich $1\Box$

(square lattice) and disk-rich 1Δ (triangular lattice) solid solutions along with the hexatic (in disk-rich region) and tetratic (in square-rich region) mesophases. The disk-rich 1Δ solid phase dissolves up to 30% of squares which do not have any orientational preference and are randomly distributed throughout the underlying 1Δ lattice sites (Fig. S3 Sec. V). The square-rich side, the $1\square$ solid phase is also able to dissolve up to 30% of disks and is preceded by the stable regions of tetratic and I phases at lower pressures. For $P^* < 18$ and for all x_s values, we observed two main phase transitions: $I \rightarrow$ hexatic and hexatic $\rightarrow 1\Delta$ solid in the disk-rich region ($x_s < 0.3$) and $I \rightarrow$ tetratic and tetratic $\rightarrow 1\square$ solid in the square-rich region ($x_s > 0.7$). The transitions from the disordered I phase to the ordered 1Δ (or $1\square$) solid, occurring through an intermediate hexatic (or tetratic) mesophase are analogous to the well-studied phase transitions in the systems of pure monodisperse hard-disks (or hard-squares). The tetratic mesophase formed by the pure squares ($x_s=1.0$) is stable over a range $\sim 8.25 < P^* < 15.4$ [21] that is wider than the $7.59 < P^* < 7.7$ [29] range of the hexatic mesophase formed by pure disks ($x_s=0$), a difference that can be attributed to the defects being more delocalized in the tetratic phase [21]. We found that, with increasing molar fraction of squares (disks) in the disk-rich (square-rich) region, the range of P^* where the hexatic (tetratic) phase is stable increases significantly compared to the pure disk (square) system. This increase in the stability region for the hexatic phase with x_s suggests that the squares accentuate the hexatic behavior as it persists even for up to $P^* \sim 16.2$, which is approximately twice the hexatic $\rightarrow 1\Delta$ solid transition pressure of $P^* \approx 7.7$. The tetratic phase is stable up to $P^* \approx 18.9$ with increasing disk concentration, which is about 1.2 times the pure-square tetratic $\rightarrow 1\square$ solid transition pressure, $P^* \approx 15.4$. This increase in the stability regions of the hexatic and tetratic phases associated with significant content of the guest component is attributable to the increased concentration of topological defects created by the dissimilarly-shaped particles residing in the host-solid lattices. These defects tend to destroy the quasi-long-range positional correlation in the solid phases, hence driving the stability of the hexatic or tetratic mesophases to well above the pure-component mesophase \rightarrow solid phase transition pressures.

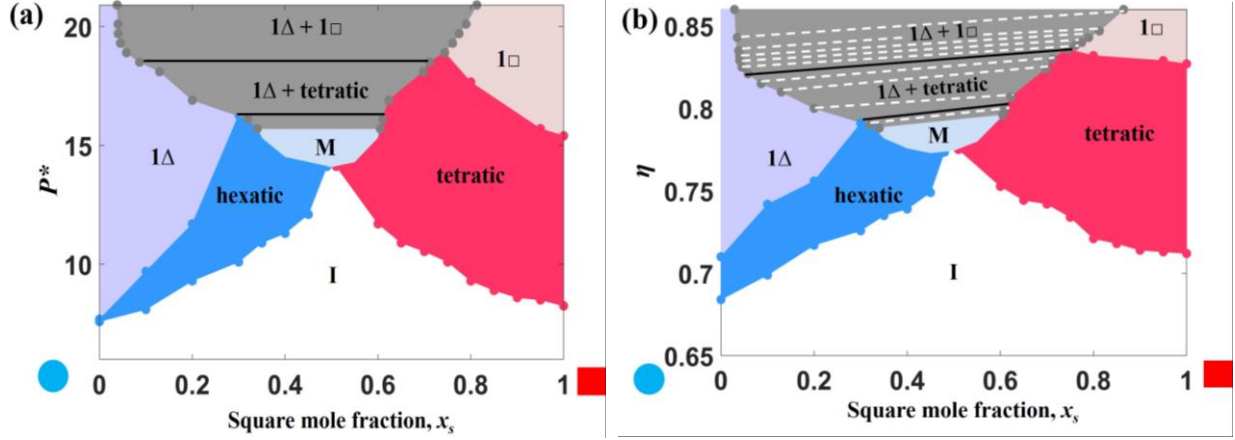


FIG. 2 (color online). Pressure-composition (a) and area fraction-composition (b) phase diagrams for mixture of disks+squares for *optimal* component size ratio, $\zeta = 1.1$. The symbols 1Δ , $1\Box$, I, and M denote the triangular solid, square solid, isotropic and the mosaic phase, respectively. The grey shaded area corresponds to the two-phase region with tie lines in (b) shown as white dashed lines.

Figure 2 shows a peculiar continuous transition between the disk-like and the square-like behaviors over a range of square molar fractions, $0.33 < x_s < 0.6$, $14.5 < P^* < 15.7$ and $0.77 < \eta < 0.8$. We assign this region bridging the hexatic and the tetratic mesophases as the mosaic (M) phase. Along increasing P^* or η , the M phase is sandwiched between the I (isotropic) and two-phase regions. We carried out interfacial simulations to minimize hysteretic effects and ascertain the conditions at which a single stable M phase region occurs. To characterize this phase, we analyzed the equation of state (EoS) (see Fig. 3a) and the six and four-fold local bond-orientational correlation functions, $g_6(r^*)$ and $g_4(r^*)$ (see Fig. 4) for $x_s = 0.5$. As can be observed in Fig. 3a, the $I \rightarrow M$ phase transition occurs at $\eta \approx 0.780$ where the global values of ψ_6 and ψ_4 increase up to 0.4-0.53, indicating significant degree of both hexatic and tetratic-like order in the system. The global Ψ_n values (where $n = 4$ or 6) are evaluated by calculating the average of the n -fold local bond orientational order, Φ_n for all particles in the system (see SI Sec. IV for details). To distinguish the M phase from the hexatic and tetratic mesophases, we examined $g_6(r^*)$, $g_4(r^*)$ and $g(r^*)$ correlation functions (see Fig. 4). At $\eta = 0.780$, the M phase showed algebraic decay of $g_6(r^*)$ and $g_4(r^*)$ with an exponent $\sim -1/4$, and short-range layering (liquid-like behavior) of $g(r^*)$. This indicates that the M phase possesses quasi-long range orientational order with both hexagonal-like and square-like structural motifs, and short-range translational order. The above results suggest that the disks and squares have comparable proclivity to form stable six-fold and four-fold ordered micro-domains,

respectively, that coexist across the system. We selected the $-1/4$ exponent as threshold to align with the KTHNY theory prediction for the scaling parameter lower-bound for the fluid to (n -fold)-atic phase transition (where $n=4$ or 6). At $P^*=16.5$ and $\eta=0.80$, the $g_6(r^*)$ and $g_4(r^*)$ curves decay faster compared to the M phase; these conditions correspond to the two-phase coexistence state containing macro-segregated six-fold and four-fold ordered domains whose bond correlation lengths are, within the given simulation box size, shorter than the M-phase quasi-long range order.

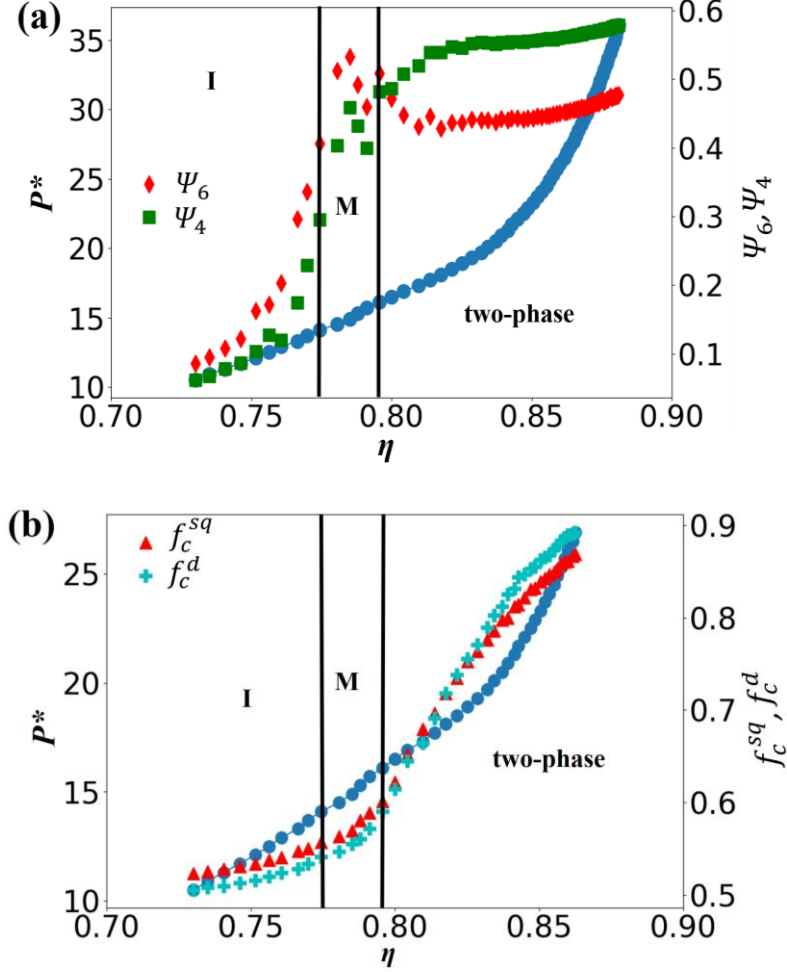


FIG. 3 (color online). Equation of state (EoS) for equimolar disks + squares mixture with $\xi = 1.1$ and $N = 1600$ (blue lines and circles) showing approximate phase boundaries and two-phase coexistence region. Besides pressure P^* , (a) shows ψ_6 (diamond) and ψ_4 (square) order parameters, and (b) shows the local composition parameters, f_c^{sq} and f_c^d , as a function of area fraction, η . I = isotropic phase; M = mosaic mesophase.

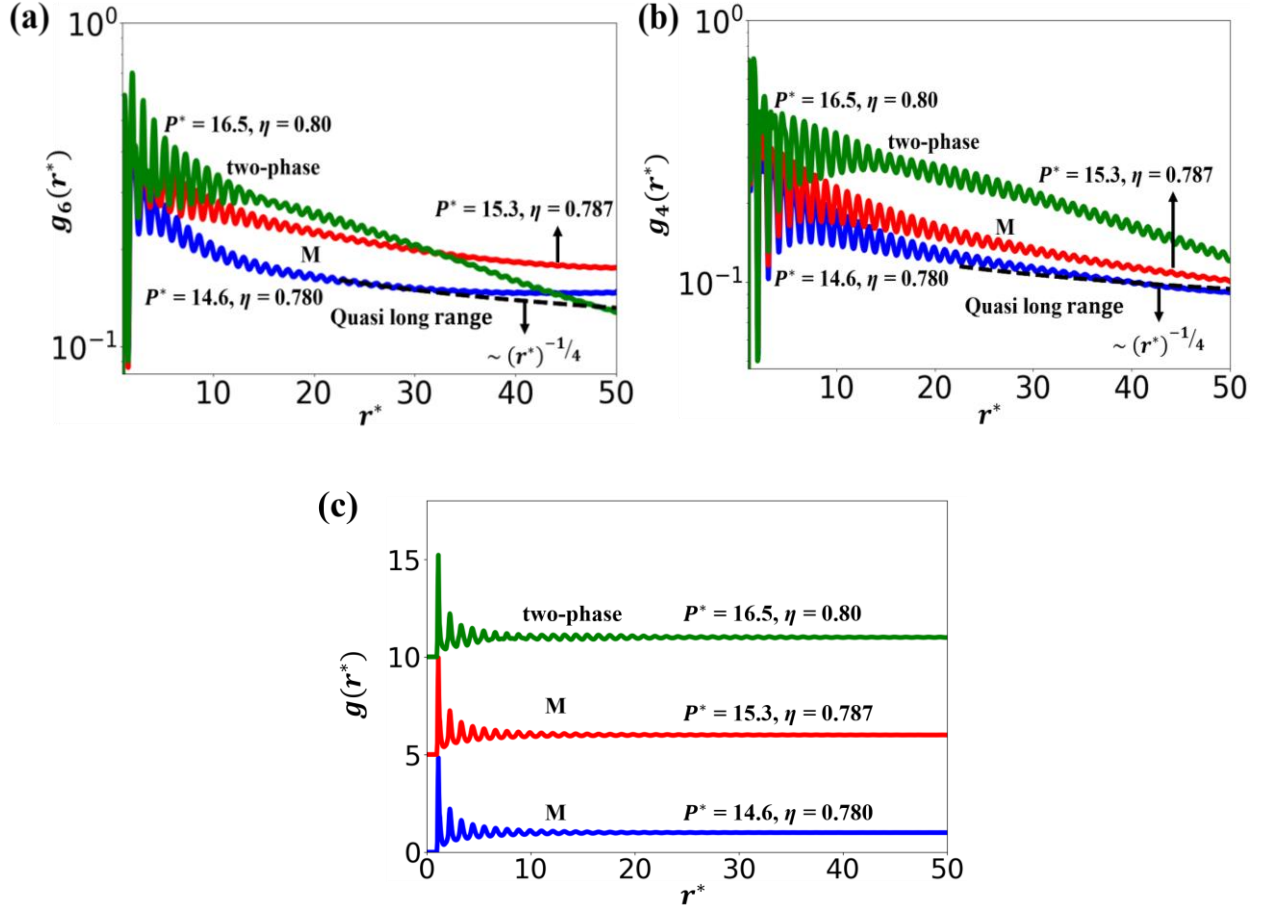
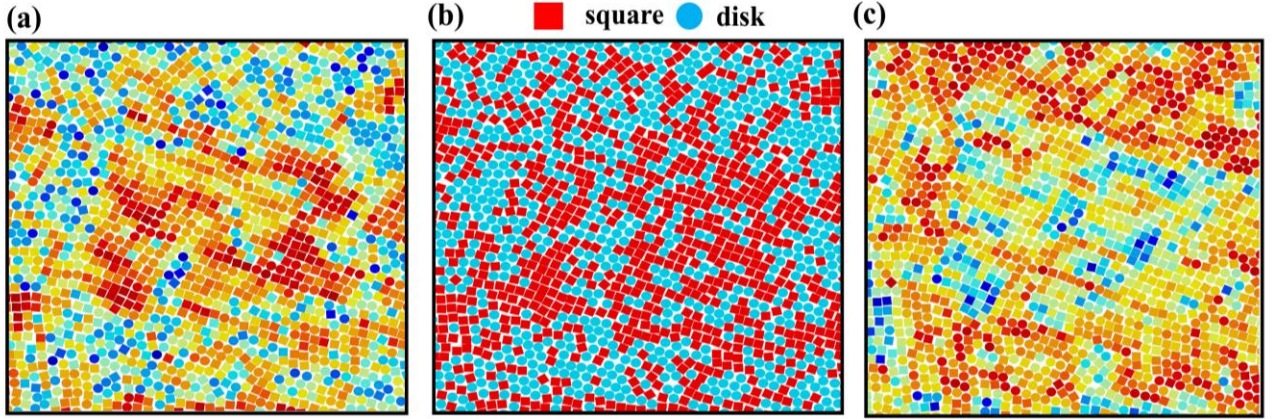


FIG. 4 (online color). Correlation functions for the equimolar disk+square mixture with $\xi = 1.1$ and $N = 12,048$ particles. Bond orientational order functions $g_6(r^*)$ (a) and $g_4(r^*)$ (b) for the isotropic (I) and mosaic (M) phases. The dashed line indicates algebraic decay of the orientational correlation with an exponent $\sim -1/4$. (c) 2D pair correlation functions shifted uniformly to distinguish peaks for the phases and conditions indicated (by pressures, P^* and area fraction, η).

Figures 5b and 5e show configurations of the M phase and the two-phase coexistence state at $P^* = 14.9$ and $\eta = 0.783$, and $P^* = 16.5$ and $\eta = 0.80$, respectively. The clusters of six-fold and four-fold ordered domains are shown by coloring the particles based on the local values of Φ_4 (Figs. 5a and 5d) and Φ_6 (Figs. 5c and 5f). For the M phase, the coloring reveals a complementary correlation between the disk-rich regions with high six-fold domains and square-rich regions with high four-fold ordered domains, that are randomly distributed throughout the simulated domain. We also detected regions of RB order formed by squares with high local values of Φ_6 . To test that the M phase is not just a system that has become kinetically arrested *in route* to macro-phase separation,

we simulated a system started at a state of complete phase separation of squares and disks at $P^*=14.9$, and confirmed that the macro-domains gradually disintegrated to form the M phase micro-domains. Movie 1 in the SI shows this transition upon decreasing P^* . Overall, our analysis indicates that the M phase is indeed a mesophase having a heterogeneous microstructure resembling a “mosaic” of different ordered micro-domains corresponding to tetratic/RB-like and hexatic-like regions.

mosaic phase



two-phase coexistence

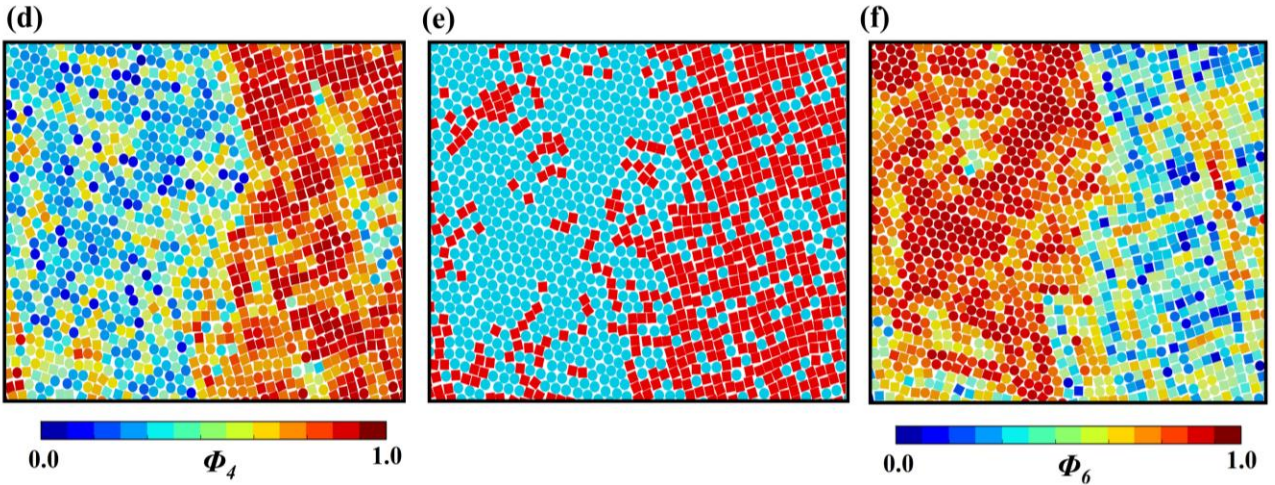


Fig. 5 (color online). Local distribution of the n -fold ($n=4, 6$) bond orientational order for the equimolar disks+squares mixture with $N=12,048$ and $\xi=1.1$. Each snapshot represents a section that is $\sim 1/10^{\text{th}}$ of the entire simulation box. Results from MC-*NPT* simulations for the mosaic phase at $P^*=14.9$, $\eta=0.783$ (top panel) and two-phase coexistence state at $P^*=16.5$, $\eta=0.8$ (bottom panel). Particles are colored based on the local values of Φ_4 (a and d) and Φ_6 (c and f).

To understand the mechanism associated with the I \rightarrow M phase transition, we computed the local composition parameters, f_c^{sq} and f_c^d to detect the correlation between the local compositional heterogeneity and the presence of ordered domains formed by squares and disks (see Fig. 3b). Parameters f_c^{sq} and f_c^d are the average fraction of the like-shaped nearest neighbor to a square and disk, respectively (normalized such that particles with all like-shaped neighbors corresponds to 1). For the I phase, the average values of both f_c^{sq} and f_c^d are close to a well-mixed value of 0.5, reflecting the overall equimolar composition. When the system is compressed to the M phase, both f_c^{sq} and f_c^d increase for $\eta > 0.77$, gradually at first and then more steeply as the solid-solid phase separated region is reached ($\eta > 0.79$ for $P^* > 15.7$). The loss of the particles' local compositional mixing observed in the M phase compared to the I phase, reveals that the entropic bonding [34,35], which favors contacts between like-shaped particles, becomes sufficiently strong to seed the formation of disk-rich hexatic and square-rich tetratic/Rhombic micro-domains. The grain boundaries around these ordered micro-domains contain particles with both f_c^{sq} and f_c^d values close to 0.5, which can be viewed as compositional “defects” contributing to the structural disorder in the M phase. The migration of these defects was monitored at $\eta = 0.783$ using “*pseudo dynamic*” Monte Carlo simulations in the *NVT* ensemble with only translation and rotation moves allowed. Movie 2 in the SI shows that, although the migration of these defects is restricted to the grain boundary regions due to the low overall translation mobility in the system, their compositions decorrelate much faster those of particles inside ordered domains (see Fig. S9c Sec. VII). This suggests that both the growth of ordered M domains from the I state and the slow restructuring of the M domain patterns would be mediated by the accrual of local rearrangements at the grain boundaries.

The overall mixing entropy of the M phase, while lower than that in the I phase (where nearly ideal mixing of components occurs), must be significant given the “*random*” mixing of the ordered clusters formed by the like-shaped particles throughout the system; i.e., while limited mixing happens at the length scale of individual particles inside clusters (as in the solid solutions) and at the grain boundaries, mixing also occurs at the length scale of the ordered clusters. The result is a system with transient but well-defined *micro*-phase segregated regions which is quite distinct to the *macro*-phase segregated state observed at higher densities and pressures. We posit that this unique mesophase behavior engenders when, at a suitable range of compositions and densities, the

two competing entropic forces, namely, entropic bonding favoring the clustering of like-particle contacts (attraction) and mixing entropy favoring random contacts, are in such a close balance that are able to coexist by attaining a “*compromise*” state exhibiting both segregated domains and random mixing of those domains. As the M phase is compressed to a higher density, the entropic cost of unlike contacts overpowers any gain in mixing entropy, leading to the phase separation of the individual components into disk-rich and square-rich ordered phases. Conceptually, the transitions $I \rightarrow M \rightarrow \text{two-solid-phases}$ with pressure for an equimolar mixture could be seen as the coarsening in the correlation length of the ordered domains, which goes from being very short ranged (I phase), to mesoscopic (M phase) to macroscopic (two-phase state). Entropically driven demixing transition in hard-core mixtures can be approximately described using a simple lattice-gas model that also incorporates a nearest neighbor entropic attraction of like-particles. One such model was effective in describing the first-order demixing transition of binary mixtures of hard squares from the I phase [36].

To underscore the importance of the optimal component size ratio, ζ , in promoting solid solution behavior and the formation of the novel M phase region, we also simulated phase diagrams for other ζ values. We varied the ζ values by $\pm 27\%$ from the representative optimal value of 1.1 so that the associated ΔF_x values are significantly higher than those in the relatively flat region for $1.04 < \zeta < 1.2$ (see Fig. S2 in SI Sec. III) where systems would be expected to exhibit a similar phase behavior. Specifically, Figure 6 shows results for $\zeta = 0.8$ and 1.4 for which, unlike the $\zeta = 1.1$ case in Fig. 2a, no M phase region was detected. In both cases, the stability region of the hexatic phase is much narrower compared to the $\zeta = 1.1$ case, as the two-phase coexistence region becomes entropically more favorable at a pressure (see P_{CO}^* in Table S2 in SI Sec. VIII) which is closer to the order-disorder transition pressure (ODP) value of pure disks. Furthermore, while for the $\zeta = 1.1$ case both the disk-rich and square-rich mesophases and solid solution regions are large and relatively comparable in size (giving the phase diagram a symmetric look), those regions become very asymmetric for the other ζ values; i.e., the hexatic and 1Δ regions are small, especially for the $\zeta = 0.8$ case. These results clearly show that a system with a (near) optimal choice of ζ promotes the stability of ordered phases with substitutional disorder over wider ranges of composition and pressure and, by construction of ΔF_x [see Eq. (1)], it does so in a way that *both* pure-component ordered phases are similarly represented. In other words, the microscopic substitutional symmetry favored by a minimal ΔF_x gets translated into a macroscopic symmetry in the substitutionally

disordered solids and mesophases in the phase diagram. These results for different ζ values can also be rationalized by their correlation with the difference between pure component ODPs or ΔODP (see Table S2 in SI Sec. VIII): as shown in Ref. [21,29], a smaller $|\Delta\text{ODP}|$ is associated with a better synchronization along the pressure scale of the tendencies of both component to order, which is conducive to more symmetric phase diagrams.

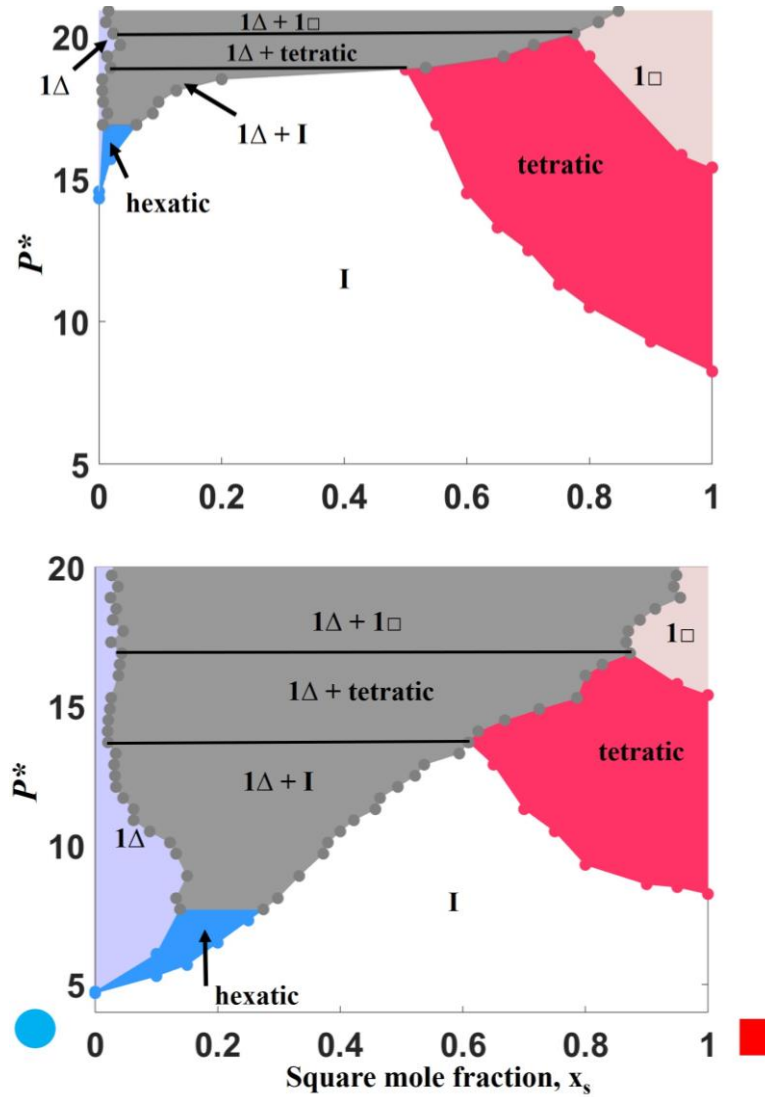


FIG. 6 (color online). Pressure-composition phase diagrams for disks (diameter σ) and squares (side edge a) with different size ratios, $\zeta = \sigma/a$. Top: $\zeta = 0.8$, Bottom: $\zeta = 1.4$. 1Δ = triangular solid, $1\square$ = square solid, and I = isotropic phase. The grey shaded area corresponds to the two-phase region with tie lines (dashed) connecting the points at the coexistence.

While the competition between 1Δ /hexatic and $1\square$ /tetratic ordering is not uncommon in 2D or quasi-2D systems, states resembling the M phase have only been seen under very restrictive

conditions. For example, cuboctahedral nanoparticles pinned at 2D fluid-fluid interfaces have been observed to transition from a hexagonal to a square lattice as surface ligands are removed and particles bond through their $\langle 100 \rangle$ facets [37]. The hexatic/tetratic like patches were observed during a transient, non-equilibrium process governed by chemical and energetic interactions. 2D simulations of hard rounded squares [38] of a particular degree of roundedness (and at a narrow range of concentrations) have predicted the formation a “*polycrystalline*” phase with a patchy-domain structure loosely reminiscent to that of the M phase. Through the rounding of square-corners, such a system could be seen as providing a physical interpolation (in a single-component system) between disks and squares to reach a state where the entropic tendencies toward the formation of hexagonal and square lattices are in close balance, like that achieved in the M phase by our disks+squares binary mixture. Mixtures such as ours, however, appear to be a more convenient platform to try to experimentally realize such a novel type of micro-phase segregated 2D phase.

In summary, we found a novel mosaic (M) phase for the disks+squares mixture, where the individual components favor distinct lattice symmetries. This M phase formed a contiguous bridge between the disk-rich hexatic region and the square-rich tetratic region and was observed only when the component size ratios were optimized to obtain maximum miscibility in their respective solid phases. It would be interesting to find out what photonic or optical properties the M phase possesses by virtue of its dual crystallinity, and whether these properties could be leveraged for applications, e.g., to fabricate a synthetic Chameleon skin [39] or optical biosensors [40]. The methods used and principles unveiled here should be general and expected to help predicting novel mesophasic behavior in other mixtures of particle shapes (as illustrated here for the disks+hexagons mixture, a case of compatible components’ crystal lattices, which exhibited a well-mixed hexatic mesophase and a 1Δ solid solution for all compositions).

Acknowledgement

Funding support from NSF award CBET-1907369 is gratefully acknowledged. The authors thank Yangyang Sun, Abhishek Sharma, Ankita Mukhtyar, and Isabela Quintela Matos for useful exchanges.

References:

- [1] J. Henzie, M. Grünwald, A. Widmer-Cooper, P. L. Geissler, and P. Yang, *Nat. Mater.* **11**, 131 (2012).
- [2] D. Seo, C. P. Ji, and H. Song, *J. Am. Chem. Soc.* **128**, 14863 (2006).
- [3] S. J. Penterman, A. Singh, W. R. Zipfel, and C. M. Liddell Watson, *Adv. Opt. Mater.* **2**, 1024 (2014).
- [4] S. Badaire, C. Cottin-Bizonne, J. W. Woody, A. Yang, and A. D. Stroock, *J. Am. Chem. Soc.* **129**, 40 (2007).
- [5] C. J. Hernandez and T. G. Mason, *J. Phys. Chem. C* **111**, 4477 (2007).
- [6] U. Agarwal and F. A. Escobedo, *Nat. Mater.* **10**, 230 (2011).
- [7] S. C. Glotzer and M. J. Solomon, *Nat. Mater.* **6**, 557 (2007).
- [8] Y. Min, M. Akbulut, K. Kristiansen, Y. Golan, and J. Israelachvili, *Nat. Mater.* **7**, 527 (2008).
- [9] Y. F. Lim, J. J. Choi, and T. Hanrath, *J. Nanomater.* **2012**, 393160 (2012).
- [10] G. Von Freymann, A. Ledermann, M. Thiel, I. Staude, S. Essig, K. Busch, and M. Wegener, *Adv. Funct. Mater.* **20**, 1038 (2010).
- [11] A. V. Kabashin, P. Evans, S. Pastkovsky, W. Hendren, G. A. Wurtz, R. Atkinson, R. Pollard, V. A. Podolskiy, and A. V. Zayats, *Nat. Mater.* **8**, 867 (2009).
- [12] C. Novo, A. M. Funston, and P. Mulvaney, *Nat. Nanotechnol.* **3**, 598 (2008).
- [13] C. R. Henry, *Catal. Letters* **145**, 731 (2015).
- [14] Z. Y. Zhou, N. Tian, J. T. Li, I. Broadwell, and S. G. Sun, *Chem. Soc. Rev.* **40**, 4167 (2011).
- [15] J. H. Conway, Y. Jiao, and S. Torquato, *Proc. Natl. Acad. Sci. U. S. A.* **108**, 11009 (2011).
- [16] G. Bautista-Carbajal, P. Gurin, S. Varga, and G. Odriozola, *Sci. Rep.* **8**, 8886 (2018).
- [17] S. Torquato and Y. Jiao, *Nature* **460**, 876 (2009).
- [18] M. R. Khadilkar and F. A. Escobedo, *Soft Matter* **12**, 1506 (2016).

- [19] P. F. Damasceno, M. Engel, and S. C. Glotzer, *ACS Nano* **6**, 609 (2012).
- [20] E. G. Teich, G. Van Anders, D. Klotsa, J. Dshemuchadse, and S. C. Glotzer, *Proc. Natl. Acad. Sci. U. S. A.* **113**, E669 (2016).
- [21] J. A. Anderson, J. Antonaglia, J. A. Millan, M. Engel, and S. C. Glotzer, *Phys. Rev. X* **7**, 021001 (2017).
- [22] X. Ye, J. E. Collins, Y. Kang, J. Chen, D. T. N. Chen, A. G. Yodh, and C. B. Murray, *Proc. Natl. Acad. Sci. U. S. A.* **107**, 22430 (2010).
- [23] E. K. Riley and C. M. Liddell, *Langmuir* **26**, 11648 (2010).
- [24] W. J. Baumgardner, K. Whitham, and T. Hanrath, *Nano Lett.* **13**, 3225 (2013).
- [25] W. H. Evers, B. Goris, S. Bals, M. Casavola, J. De Graaf, R. Van Roij, M. Dijkstra, and D. Vanmaekelbergh, *Nano Lett.* **13**, 2317 (2013).
- [26] B. Liu, T. H. Besseling, M. Hermes, A. F. Demirörs, A. Imhof, and A. Van Blaaderen, *Nat. Commun.* **5**, 3092 (2014).
- [27] W. H. Evers, J. M. Schins, M. Aerts, A. Kulkarni, P. Capiod, M. Berthe, B. Grandidier, C. Delerue, H. S. J. Van Der Zant, C. Van Overbeek, J. L. Peters, D. Vanmaekelbergh, and L. D. A. Siebbeles, *Nat. Commun.* **6**, 8195 (2015).
- [28] M. Danek, K. F. Jensen, C. B. Murray, and M. G. Bawendi, *Chem. Mater.* **8**, 173 (1996).
- [29] E. P. Bernard and W. Krauth, *Phys. Rev. Lett.* **107**, 155704 (2011).
- [30] J. A. Millan, D. Ortiz, G. Van Anders, and S. C. Glotzer, *ACS Nano* **8**, 2918 (2014).
- [31] J. Russo and N. B. Wilding, *Phys. Rev. Lett.* **119**, 115702 (2017).
- [32] A. Buhot and W. Krauth, *Phys. Rev. E* **59**, 2939 (1999).
- [33] F. A. Escobedo, *J. Chem. Phys.* **146**, 134508 (2017).
- [34] G. Van Anders, N. K. Ahmed, R. Smith, M. Engel, and S. C. Glotzer, *ACS Nano* **8**, 931 (2014).
- [35] G. Van Anders, D. Klotsa, N. K. Ahmed, M. Engel, and S. C. Glotzer, *Proc. Natl. Acad. Sci. U. S. A.* **111**, E4812 (2014).
- [36] D. Frenkel and A. A. Louis, *Phys. Rev. Lett.* **68**, 3363 (1992).
- [37] K. Whitham and T. Hanrath, *J. Phys. Chem. Lett.* **8**, 2623 (2017).
- [38] C. Avendaño and F. A. Escobedo, *Soft Matter* **8**, 4675 (2012).
- [39] J. Teyssier, S. V. Saenko, D. Van Der Marel, and M. C. Milinkovitch, *Nat. Commun.* **6**, 6368 (2015).
- [40] S. V. Boriskina and L. Dal Negro, *Opt. Express* **16**, 12511 (2008).